Journal of Alloys and Compounds 868 (2021) 159252

Contents lists available at ScienceDirect

Journal of Alloys and Compounds

journal homepage: www.elsevier.com/locate/jalcom

Speed enhancement of ultraviolet photodetector base on ZnO quantum dots by oxygen adsorption on surface defects

Hongyu Ma[a,b], Kewei Liu[a,b,*], Zhen Cheng[a], Zhiyao Zheng[a,b], Yinzhe Liu[a,b], Peixuan Zhang[a,b], Xing Chen[a,b], Deming Liu[a], Lei Liu[a,b], Dezhen Shen[a,b,*]

[a] State Key Laboratory of Luminescence and Applications, Changchun Institute of Optics, Fine Mechanics and Physics, Chinese Academy of Sciences, Changchun 130033, China
[b] Center of Materials Science and Optoelectronics Engineering, University of Chinese Academy of Sciences, Beijing 100049, China

ARTICLE INFO

Article history:
Received 8 February 2021
Accepted 17 February 2021
Available online 19 February 2021

Keywords:
ZnO
Quantum dots
Ultraviolet photodetector
Oxygen vacancy

ABSTRACT

Applications of ZnO quantum dots (QDs) in photodetectors are generally limited by a slower response speed and a higher dark current. The corresponding mechanism is not very clear, and how to resolve these problems is still in big challenge. Herein, we have demonstrated a photodetector on 700 nm-thick ZnO QDs film with a large number of oxygen vacancy defects by adjusting the ratio of the reactants and the reaction time. The device exhibits a quick response speed with a rise time of ~1.00 s and a recovery time of ~0.19 s. Meanwhile, the dark current and the responsivity under 730 μW/cm^2 UV light illumination were found to be 20 pA and 260 mA/W under 10 V bias, respectively. The mechanism of these phenomena has been investigated, and the fast response speed of ZnO QDs photodetector in the air should originate from the adsorption/desorption of oxygen on the surface oxygen vacancy defects of ZnO QDs. The findings in this work can be used to guide design of high-performance photodetectors based on ZnO QDs and other nanomaterials with large surface to volume ratio.

1. Introduction

Ultraviolet (UV) photodetectors have been widely applied both in civilian and military areas, such as high temperature flame detection, missile launching detection, environmental monitoring, optical communications and so on [1–5]. Owing to the extreme radiation hardness, intrinsic visible blindness and strong UV absorption, wide band gap semiconductors, including ZnO, GaN, SiC, etc., have been regarded as ideal materials for the UV detection [6–9]. In recent years, quantum dots (QDs) or nanoparticles have attracted more and more attention due to their strong light absorption, size-tunable bandgaps and low-cost and simple fabrication, which are beneficial to the application of photodetection. Among different wide band gap semiconductors, ZnO has many special advantages, such as wide direct band gap (3.37 eV), low defect density, high saturated carrier drift rate, rich in raw materials and environmentally friendly [10–19]. More importantly, ZnO exhibits the most diverse and abundant configurations of nanostructures [20–24], and QDs are a typical representative among them. Till now, the UV photodetectors based on ZnO QDs have been widely investigated, and relatively high responsivity was commonly observed. The inherent interfacial barrier between the connected ZnO QDs is considered to be the main reason for the increase in UV response. However, the reported pure ZnO QDs UV photodetectors usually suffered from the low response speed and the large dark current. Although the performance of ZnO QDs UV photodetectors can be effectively improved by introducing graphene [25], carbon dots [26] and metal particles [27–30] the relatively complicated process and the increase in cost will undoubtedly hinder its large-scale application.

Here, we report a solution-processed ZnO QDs UV photodetector on sapphire substrates with Au interdigitated electrodes. A stable switching behavior with high photo-to-dark current ratio, and fast response and recovery speed has been demonstrated. X-ray photoelectron spectroscopy (XPS) analysis, photoluminescence (PL) and PL excitation (PLE) spectra, and the time-dependent photocurrent measurements in vacuum and air atmosphere suggested that the large amounts of oxygen vacancy (V_O) surface defects and the adsorption/desorption of oxygen molecules on them should be responsible for

* Corresponding authors at: State Key Laboratory of Luminescence and Applications, Changchun Institute of Optics, Fine Mechanics and Physics, Chinese Academy of Sciences, Changchun 130033, China.
E-mail addresses: liukw@ciomp.ac.cn (K. Liu), shendz@ciomp.ac.cn (D. Shen).

https://doi.org/10.1016/j.jallcom.2021.159252
0925-8388/

the fast response speed. Our findings in this work pave the way for developing low-cost high-speed ZnO-based photodetectors.

2. Experimental details

2.1. Preparation of ZnO QDs

At first, 1.1 g (5 mmol) $Zn(CH_3COO)_2.2\ H_2O$ was added into 30 mL absolute ethanol under continuous stirring at 70 °C for 1 h. Then the solution was cooled down to 0 °C in an ice water bath. At the same time, 0.41 g (7 mmol) KOH was dissolved in 3 mL absolute ethanol, which was then slowly added into the solution of Zn $(CH_3COO)_2.2\ H_2O$. The mixed solution changed from turbidity to clear in only a few seconds. After that, n-Hexane (about 3 times of the ethanol with ZnO QDs by volume) was immediately added into the mixed solution, and then ZnO QDs were obtained as precipitate. The precipitate was collected and washed with ethanol for three times. Finally, ZnO QDs were re-dispersed into absolute ethanol with a concentration of 1 mol L^{-1}.

2.2. Fabrication of ZnO QDs photodetector

c-face sapphire was selected as the substrate, which was cleaned by ultrasonic agitation with trichloroethylene, acetone and ethanol sequentially. Then the Au interdigital electrodes with 10 μm in width, 500 μm in length and 10 μm in space were made on sapphire substrate by using the traditional photolithography and lift-off techniques. Sequentially, ZnO QDs solution was spin-coated on the substrate with Au interdigital electrodes at a rotation rate of 2000 rpm for 20 s. After that, the sample was dried on a hotplate at 90 °C for 1 min. The abovementioned process was repeated three times to obtain 700-nm-think dense QDs film.

2.3. Characterizations of the materials and devices

The morphology and the crystal structure of the ZnO QDs and their film were characterized by transmission electron microscopy (TEM) (FEI Talos F200s), scanning electron microscope (SEM) (HITACHI S-4800) and X-ray diffraction (XRD) (Rigaku) with Cu Kα as the radiation source (λ = 0.154 nm). PL and PLE spectra were analyzed by a fluorescence spectrophotometer (HitachiF-7000). XPS measurements were performed using a commercial XPS spectrometer (Thermo ESCALAB 250). The absorption spectra were obtained at room temperature by using a UV-3101PC scanning spectrophotometer. Current-Voltage (*I-V*) and time-dependent photocurrent (*I-t*) measurements of the photodetector were carried out by a semiconductor parameter analyzer (Keithely 2200). The response spectra were measured by using a 200 W UV-enhanced Xe lamp and a monochromator.

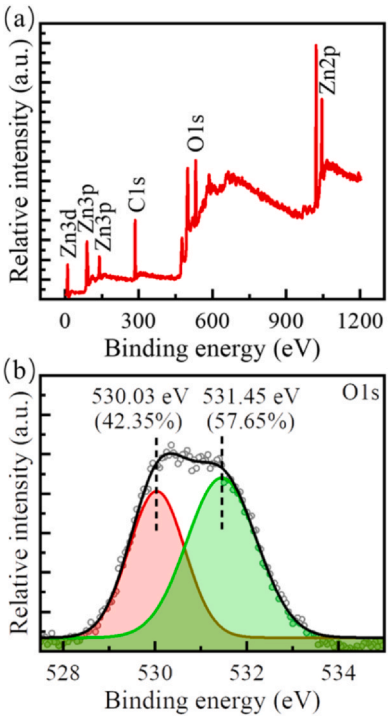

Fig. 2. (a) The evolution of XPS survey spectra of ZnO QDs film in a full 1200 eV binding energy range. (b) The evolution of XPS O1s core level lines of ZnO QDs film.

3. Results and discussion

Fig. 1a depicts a typical TEM image of the ZnO QDs, indicating that the size of ZnO QDs is highly uniform with a diameter of about 4 nm. Fig. 1b shows XRD pattern of ZnO QDs. The diffraction peaks located at 31.7°, 36.2°, 47.5°, 56.5° and 62.7° can be indexed to (100), (101), (102), (110) and (103) planes of wurzite-type ZnO (JCPDS 36–1451). PL and PLE spectra of ZnO QDs solution are shown in Fig. 1c. The room temperature PL spectrum under the UV excitation (λ = 325 nm) by a lamp exhibits a weak UV peak at 3.40 eV (365 nm) and a broad green-emission band peaked at about 2.28 eV (544 nm). The PLE spectrum monitored at 550 nm emission has a sharp peak at 3.46 eV. The UV emission can be attributed to the near-band-edge excitonic recombination of ZnO, while the visible emission is quite generally considered to be the result of radiative recombination of photo-generated holes with singularly ionized oxygen vacancies. So, the weak UV emission and the strong visible emission suggest that our ZnO QDs have lots of V_O defects [31].

The XPS spectrum of ZnO QDs film spin-coated on a sapphire substrate in the full binding energy (BE) range from 0 to 1200 eV is shown in Fig. 2a. The binding energies are calibrated by taking the carbon C1s peak (284.6 eV) as reference[32]. All the peaks can be

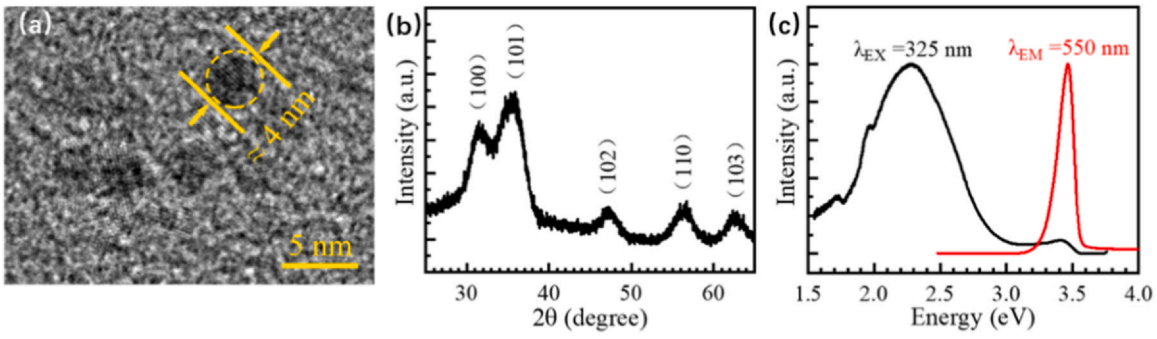

Fig. 1. (a) TEM image, (b) XRD pattern, (c) PL and PLE spectra of ZnO QDs.

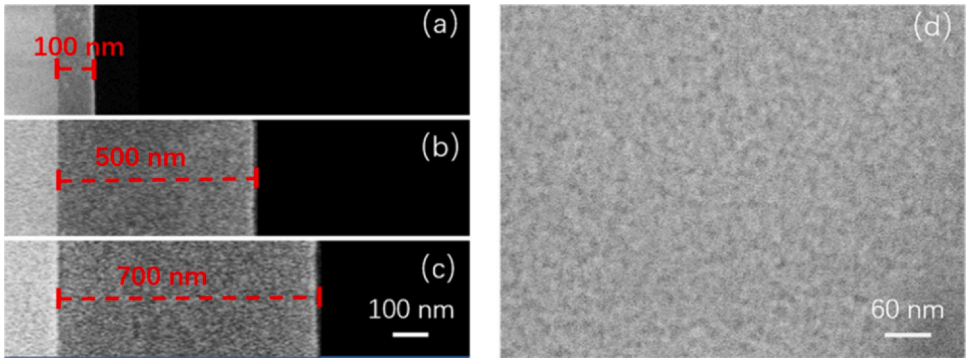

Fig. 3. (a-c) Cross-sectional SEM images of ZnO QDs films on sapphire substrate spin-coated once, twice and three times, respectively. (d) Top-view SEM image of ZnO QDs films.

ascribed to Zn, O, and C, as labeled in Fig. 2a. Moreover, XPS O1s line, as a crucial point of our studies, is shown in Fig. 2b. The curve exhibits an evident asymmetry and the deconvolution was performed by using the Gauss fitting. Obviously, the O1s peak can be decomposed into two components at 530.03 eV and 531.45 eV. The low-energy peak at 530.03 eV can be attributed to lattice oxygen in wurzite-type ZnO. And the peak at 531.45 eV is associated with the oxygen deficient regions on the surface of ZnO [33]. It is worth noting that, two observed oxygen peaks at 530.03 eV and 531.45 eV accounted for 42.35% and 57.65% of the total O1s area, respectively, further confirming the large amounts of oxygen-deficient states on the ZnO QDs surface.

Fig. 3a-c show the SEM cross-sectional views of ZnO QDs films on sapphire substrate spin-coated once, twice and three times, respectively. And Fig. 3d presents the SEM top view of ZnO QDs films. It can be found that ZnO QDs film is very uniform and flat. And with the increase of spin-coating numbers, the thicknesses of ZnO QDs films increase from 100 nm to 700 nm.

Fig. 4 shows the UV–vis absorption spectrum of ZnO QDs spin-coated on sapphire substrate. The absorption spectrum has a steep absorption edge near 360 nm, and the corresponding bandgap of the ZnO QDs is ~3.46 eV, as shown in the inset of Fig. 4. The absorption spectrum of ZnO QDs film is in full compliance with PLE of ZnO QDs solution, indicating that the 90 °C heat treatment hardly changes the size of ZnO QDs.

In order to investigate the photoresponse properties of the ZnO QDs, the metal-semiconductor-metal (MSM) photodetector based on ZnO QDs film with a thickness of 700 nm has been demonstrated (see the left inset of Fig. 5a). Fig. 5a shows the responsivity of the device as a function of the incident light wavelength at a bias of 10 V. For wavelength shorter than 365 nm, the device shows a high responsivity, and the highest value is about 0.26 A/W. And then the responsivity of the device drops and reaches its lowest value at the wavelength of about 400 nm. The UV/visible rejection ratio ($R_{350\,nm}$/

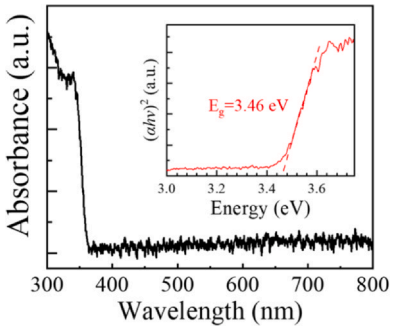

Fig. 4. Room temperature UV–vis absorption spectrum of ZnO QDs film spin coated on a sapphire substrate. The inset shows the variation of $(\alpha h\nu)^2$ versus the photo energy ($h\nu$).

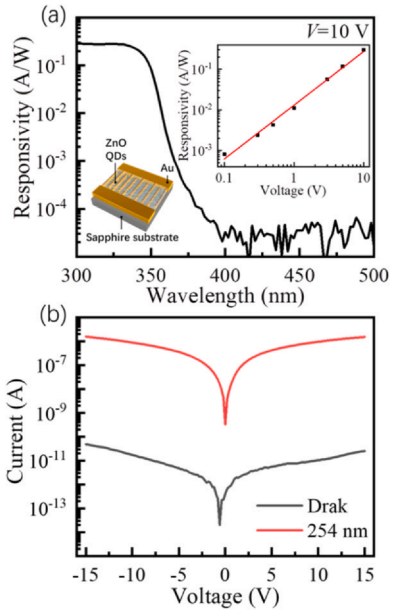

Fig. 5. (a) The spectral response of the ZnO QDs detector under 10 V applied bias. The insets show the structure of ZnO QDs detector and the variation of responsivity versus the applied bias. (b) I–V curves of the ZnO QDs detector both in dark and under 254 nm illumination.

$R_{400\,nm}$) is nearly 10^5, indicating the intrinsic visible-blind characteristics of the ZnO QDs photodetector. Besides, as shown in the right inset of Fig. 5a, the responsivity of device increases nearly linearly with the increase of bias voltage from 0.1 V to 10 V. Fig. 5b shows the semi-logarithmic I-V curves of the device in the dark and under UV illumination (λ = 254 nm, p = 730 μW/cm^2) at room temperature. The ZnO QDs film is very resistive in the dark, and the device has a low dark current of 20 pA at 10 V bias. Meanwhile, the light-to-dark current ratio (I_{light}/I_{dark}) can be as high as over 10^4.

Fig. 6a depicts the dynamic photocurrent response of the ZnO QDs photodetector at 10 V bias under a 254 nm UV illumination with a power density of 730 μW/cm^2. As we can see, the device has excellent stability and reproducibility. Once the UV light is turned on, the current increases rapidly and reaches a steady state, achieving an enhancement of over 10^4-fold. When UV illumination is turned off, the current quickly drops to its initial level. In order to better evaluate the response speed of the device, a normalized response curve is given in Fig. 6b. The response time (τ_r) of ZnO QDs photodetector, defined as the time for the current to increase from 10% to 90% of the peak value after switching on the light, is around 1.00 s. And the decay time (τ_d), defined as the time for the current to decrease from 90% to 10% of peak value after switching off the light, is about 0.19 s. Table 1 summarizes the performance parameters of our ZnO QDs

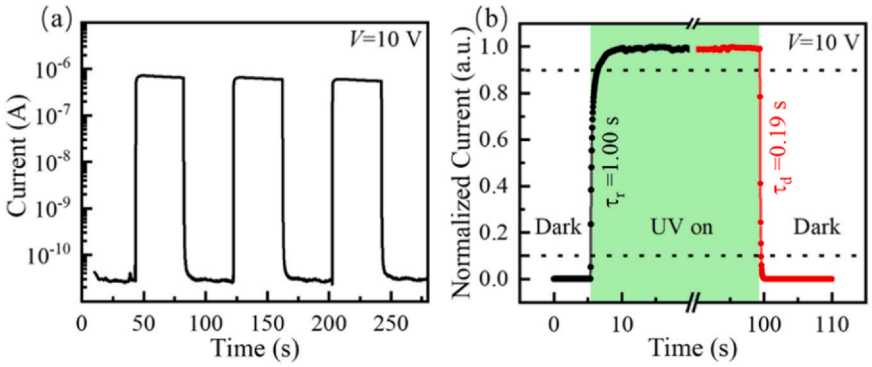

Fig. 6. (a) Time-dependent photocurrent of the photodetector by periodic switching of UV illumination (254 nm) under 10 V bias. (b) The corresponding normalized temporal photoresponse curve.

photodetector and the other recently reported photodetectors based on ZnO QDs [26–30,34–37]. It is clear that our device is extremely competitive in all aspects of performance, especially in response speed and dark current.

It is important to explain why our device has a quicker response speed. According to the previous reports, it is generally accepted that the QD-QD junction barriers are similar to back-to-back Schottky barriers (SBs), and the light-induced barrier height change is much faster than the oxygen adsorption/desorption process, which could be responsible for the quick response speed [38,39]. If this is true, the response speed of the device in vacuum should at least not be slower than in air. However, both previous reports and our results indicate that the response speed of the device in vacuum is significantly slower than in air (see Fig. S1)[35,40–42]. Therefore, besides the QD-QD junction barriers, the oxygen adsorption and desorption should also play an important role in the quick response speed.

Generally, the adsorption of oxygen occurs on the surface of ZnO, especially the oxygen vacancies [43]. Considering the large amounts of oxygen-deficient states on the ZnO QDs surface in our work, the oxygen adsorption and desorption on these surface defects should be responsible for the quick response speed of our device in air. To further confirm the effect of surface oxygen-deficient states on the response speed of the ZnO QDs photodetector, time-dependent photoresponse measurement was carried out for the devices with and without H_2O_2 solution treatment as shown in Fig. 7a. Obviously, the decay time of ZnO QDs photodetector would be dramatically increased by H_2O_2 solution treatment with an obvious persistent photoconductivity (PPC) effect. By comparing the XPS O1s core level spectra in Fig. 7b and Fig. 2b, it can be concluded that the number of V_O defects was reduced after the treatment with H_2O_2 solution. Therefore, the quick response speed of our device in air can be attributed to the oxygen adsorption and desorption on the surface oxygen vacancies of ZnO QDs.

For ZnO QDs, the chemical adsorption of oxygen causes electrons to be transferred from ZnO to the oxygen adsorbed on their surfaces. Based on the previous reports, compared with other locations on the surface, oxygen molecules as the oxidizing gas are more likely to chemically adsorb to oxygen vacancy defects [43–49]. Therefore, the adsorption of oxygen by oxygen vacancy defects contributes to the recombination of non-equilibrium carriers, thereby increasing the recovery speed of the ZnO QDs photodetector.

4. Conclusions

In summary, a ZnO QDs film photodetector has been demonstrated on the sapphire substrate with Au interdigital electrodes. Systematic investigations on the photoresponse characteristics of ZnO QDs photodetector have been carried out. The device under 254 nm wavelength illumination at 10 V showed ratios of the photocurrents to the dark currents of more than 10^4. And ZnO QDs photodetector in air exhibits a fast rise and decay times of ~1.00 s and ~0.19 s, respectively. The quick and efficient adsorption/desorption of oxygen molecules on the oxygen vacancy defects of ZnO QDs should play an important role in the fast response and recovery process. The present work would pave a new way to achieve low-cost, low dark current, and high-speed nano-structured photodetectors.

CRediT authorship contribution statement

Hongyu Ma: Idea, The main experimentation, Investigation, Writing - original draft. **Kewei Liu:** Validation, Formal analysis, Writing - review & editing, Supervision, Resources. **Zhen Cheng:** Resources, Supervision. **Zhiyao Zheng:** Experimentation supporting, Supervision. **Yinzhe Liu:** Experimentation supporting, Supervision. **Peixuan Zhang:** Experimentation supporting, Supervision. **Xing Chen:** Resources, Supervision. **Deming Liu:** Resources, Supervision. **Lei Liu:** Resources, Supervision. **Dezhen Shen:** Writing - review & editing, Supervision, Resources.

Table 1
Comparison of the characteristic parameters for various ZnO QDs-based UV detectors.

Materials	Responsivity (A/W)	Bias (V)	τ_r (s)	τ_d (s)	Dark Current (A)	Ref.
ZnO QD/C	1.7×10^6	14	–	–	–	[26]
ZnO QD/Cu	2.34×10^2	10	7.4	29	–	[27]
ZnO NP:Ni	7.52×10^{-6}	5	0.5	2	2.8×10^{-10}	[28]
ZnO QD/Al	0.779	10	2.17	0.48	–	[29]
ZnO QD/Au	0.23	10	3.55	1.49	–	[30]
ZnO QD	61	120	>25	> 120	1.5×10^{-10}	[34]
ZnO QD	–	2	1.51	36.7	2×10^{-12}	[35]
ZnO QD	–	20	411.76	322.96	3×10^{-7}	[36]
ZnO QD	–	5	250	150	3.61×10^{-9}	[37]
ZnO QD	0.26	10	1.00	0.19	3×10^{-11}	Our work

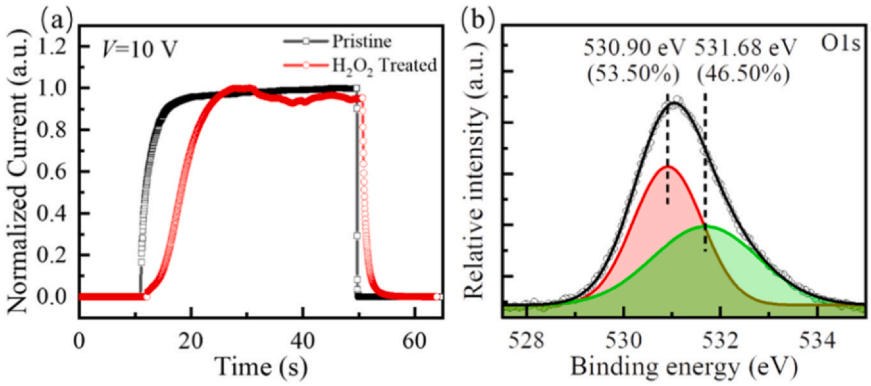

Fig. 7. (a) Time-dependent photocurrent of the devices with and without H_2O_2 solution treatment by switching on/off UV light illumination (254 nm) under 10 V bias. (b) The evolution of XPS O1s core level lines of ZnO QDs film with H_2O_2 solution treatment.

Declaration of Competing Interest

The authors declare that they have no known competing financial interests or personal relationships that could have appeared to influence the work reported in this paper.

Acknowledgements

This work is supported by the National Natural Science Foundation of China (62074148, 61475153, 61605200, 61875194, 11727902, 61425021, 61525404), Jilin Province Young and Middle-aged Science and Technology Innovation Leaders and Team Project (20180519023JH), the 100 Talents Program of the Chinese Academy of Sciences, Youth Innovation Promotion Association, CAS (2020225).

Appendix A. Supporting information

Supplementary data associated with this article can be found in the online version at doi:10.1016/j.jallcom.2021.159252.

References

[1] H.W. Lin, S.Y. Ku, H.C. Su, C.W. Huang, Y.T. Lin, K.T. Wong, C.C. Wu, Highly efficient visible-blind organic ultraviolet photodetectors, Adv. Mater. 17 (2005) 2489–2493 2489-248.
[2] Y.K. Mishra, G. Modi, V. Cretu, V. Postica, O. Lupan, T. Reimer, I. Paulowicz, V. Hrkac, W. Benecke, L. Kienle, R. Adelung, Direct growth of freestanding zno tetrapod networks for multifunctional applications in photocatalysis, uv photodetection, and gas sensing, ACS Appl. Mater. Interfaces 7 (2015) 14303–14316.
[3] D. Gedamu, I. Paulowicz, S. Kaps, O. Lupan, S. Wille, G. Haidarschin, Y.K. Mishra, R. Adelung, Rapid fabrication technique for interpenetrated zno nanotetrapod networks for fast uv sensors, Adv. Mater. 26 (2014) 1541–1550.
[4] H. Zhou, G.-J. Fang, N. Liu, X.-Z. Zhao, Effects of thermal annealing on the performance of al/zno nanorods/pt structure ultraviolet photodetector, Mater. Sci. Eng. B 176 (2011) 740–744.
[5] S.K. Shaikh, S.I. Inamdar, V.V. Ganbavle, K.Y. Rajpure, Chemical bath deposited zno thin film based uv photoconductive detector, J. Alloy. Compd. 664 (2016) 242–249.
[6] S.-H. Lim, Y.-H. Ko, C. Rodriguez, S.-H. Gong, Y.-H. Cho, Electrically driven, phosphor-free, white light-emitting diodes using gallium nitride-based double concentric truncated pyramid structures, Light Sci. Appl. 5 (2016) e16030-e16030.
[7] R. Wu, K. Zhou, C.Y. Yue, J. Wei, Y. Pan, Recent progress in synthesis, properties and potential applications of sic nanomaterials, Prog. Mater. Sci. 72 (2015) 1–60.
[8] C. Zhou, K. Liu, Y. Zhu, J. Yang, X. Chen, B. Li, Z. Zhang, D. Shen, Self-powered solar-blind ultraviolet photodetector based on au/znmgo/zno:Al with comb-shaped schottky electrode, Sens. Actuators A Phys. 295 (2019) 623–628.
[9] C. Tian, D. Jiang, J. Pei, L. Sun, R. Liu, Z. Guo, J. Hou, J. Zhao, Q. Liang, S. Gao, J. Qin, Performance enhancement of mgzno-based visible-blind photodetectors by pt nanoparticles, J. Alloy. Compd. 667 (2016) 65–68.
[10] K. Liu, M. Sakurai, M. Aono, Zno-based ultraviolet photodetectors, Sensors 10 (2010) 8604–8634.
[11] S. Pearton, D. Norton, K. Ip, Y. Heo, T. Steiner, Recent advances in processing of zno, J. Vac. Sci. Technol. B Microelectron. Nanometer Struct. 22 (2004) 932–948.
[12] D.C. Look, Recent advances in zno materials and devices, Mater. Sci. Eng. B 80 (2001) 383–387.
[13] A. Ohtomo, M. Kawasaki, Y. Sakurai, Y. Yoshida, H. Koinuma, P. Yu, Z.K. Tang, G.K.L. Wong, Y. Segawa, Room temperature ultraviolet laser emission from zno nanocrystal thin films grown by laser mbe, Mater. Sci. Eng. B 54 (1998) 24–28.
[14] S.M. Hatch, J. Briscoe, S. Dunn, A self-powered zno-nanorod/cuscn uv photodetector exhibiting rapid response, Adv. Mater. 25 (2013) 867–871.
[15] L. Li, L. Gu, Z. Lou, Z. Fan, G. Shen, Zno quantum dot decorated zn2sno4 nanowire heterojunction photodetectors with drastic performance enhancement and flexible ultraviolet image sensors, ACS Nano 11 (2017) 4067–4076.
[16] A.P. Litvin, I.V. Martynenko, F. Purcell-Milton, A.V. Baranov, A.V. Fedorov, Y.K. Gun'ko, Colloidal quantum dots for optoelectronics, J. Mater. Chem. A 5 (2017) 13252–13275.
[17] W. Tian, H. Lu, L. Li, Nanoscale ultraviolet photodetectors based on onedimensional metal oxide nanostructures, Nano Res. 8 (2015) 382–405.
[18] X. Li, X. Li, B. Zhu, J. Wang, H. Lan, X. Chen, Synthesis of porous zns, zno and zns/zno nanosheets and their photocatalytic properties, RSC Adv. 7 (2017) 30956–30962.
[19] M. Hoang Tran, T. Park, J. Hur, Solution-processed zno:Graphene quantum dot/poly-tpd heterojunction for high-performance uv photodetectors, Appl. Surf. Sci. (2021) 539.
[20] M. Chen, L. Hu, J. Xu, M. Liao, L. Wu, X. Fang, Zno hollow-sphere nanofilm-based high-performance and low-cost photodetector, Small 7 (2011) 2449–2453.
[21] A. Ghasempour Ardakani, M. Pazoki, S.M. Mahdavi, A.R. Bahrampour, N. Taghavinia, Ultraviolet photodetectors based on zno sheets: the effect of sheet size on photoresponse properties, Appl. Surf. Sci. 258 (2012) 5405–5411.
[22] H. Li, S. Jiao, H. Li, L. Li, X. Zhang, Band-edge modulated zno pomegranates-on-paper photodetector, J. Mater. Chem. C 3 (2015) 3702–3707.
[23] F. Wang, D. Zhao, Z. Guo, L. Liu, Z. Zhang, D. Shen, Artificial leaf structures as a uv detector formed by the self-assembly of zno nanoparticles, Nanoscale 5 (2013) 2864–2869.
[24] I.C. Yao, T.-Y. Tseng, P. Lin, Zno nanorods grown on polymer substrates as uv photodetectors, Sens. Actuators A Phys. 178 (2012) 26–31.
[25] D. Ick Son, H. Yeon Yang, T.W. Kim, W. Il Park, Photoresponse mechanisms of ultraviolet photodetectors based on colloidal zno quantum dot-graphene nanocomposites, Appl. Phys. Lett. (2013) 102.
[26] D.Y. Guo, C.X. Shan, S.N. Qu, D.Z. Shen, Highly sensitive ultraviolet photodetectors fabricated from zno quantum dots/carbon nanodots hybrid films, Sci. Rep. 4 (2014) 7469.
[27] M.Y. Li, M. Yu, D. Su, J. Zhang, S. Jiang, J. Wu, Q. Wang, S. Liu, Ultrahigh responsivity uv photodetector based on cu nanostructure/zno qd hybrid architectures, Small 15 (2019) 1901606.
[28] F. Abbasi, F. Zahedi, M.H. Yousefi, Fabricating and investigating high photoresponse uv photodetector based on ni-doped zno nanostructures, Opt. Commun. (2021) 482.
[29] S. Liu, M.-Y. Li, J. Zhang, D. Su, Z. Huang, S. Kunwar, J. Lee, Self-assembled al nanostructure/zno quantum dot heterostructures for high responsivity and fast uv photodetector, Nano Micro Lett. 12 (2020) 114.
[30] S. Liu, M.Y. Li, D. Su, M. Yu, H. Kan, H. Liu, X. Wang, S. Jiang, Broad-band high-sensitivity zno colloidal quantum dots/self-assembled au nanoantennas heterostructures photodetectors, ACS Appl. Mater. Interfaces 10 (2018) 32516–32525.
[31] X. Tang, E.S.G. Choo, L. Li, J. Ding, J. Xue, Synthesis of zno nanoparticles with tunable emission colors and their cell labeling applications, Chem. Mater. 22 (2010) 3383–3388.
[32] M. Kwoka, A. Kulis-Kapuscinska, D. Zappa, E. Comini, J. Szuber, Novel insight on the local surface properties of zno nanowires, Nanotechnology 31 (2020) 465705.
[33] X. Wang, Y.H. Yu, Z.L. Pei, X.D. Bai, C. Sun, R.F. Huang, L.S. Wen], X-ray photoelectron spectroscopy and auger electron spectroscopy studies of al-doped zno films, Appl. Surf. Sci. (2000).
[34] Y.Z. Jin, J.P. Wang, B.Q. Sun, J.C. Blakesley, N.C. Greenham, Solution-processed ultraviolet photodetedtors based on colloidal zno nanoparticles, Nano Lett. 8 (2008) 1649–1653.

[35] W. Yan, N. Mechau, H. Hahn, R. Krupke, Ultraviolet photodetector arrays assembled by dielectrophoresis of zno nanoparticles, Nanotechnology 21 (2010) 115501.
[36] S.K. Mishra, R.K. Srivastava, S.G. Prakash, Photoluminescence and photoconductivity studies of zno nanoparticles prepared by solid state reaction method, J. Mater. Sci. Mater. Electron. 24 (2012) 125–134.
[37] N. Nasiri, R. Bo, F. Wang, L. Fu, A. Tricoli, Ultraporous electron-depleted zno nanoparticle networks for highly sensitive portable visible-blind uv photodetectors, Adv. Mater. 27 (2015) 4336–4343.
[38] X. Xu, C. Xu, J. Hu, High-performance deep ultraviolet photodetectors based on zno quantum dot assemblies, J. Appl. Phys. 116 (2014) 103105.
[39] W. Tian, C. Zhang, T. Zhai, S.L. Li, X. Wang, M. Liao, K. Tsukagoshi, D. Golberg, Y. Bando, Flexible sno(2) hollow nanosphere film based high-performance ultraviolet photodetector, Chem. Commun. 49 (2013) 3739–3741.
[40] S.-E. Ahn, H.J. Ji, K. Kim, G.T. Kim, C.H. Bae, S.M. Park, Y.-K. Kim, J.S. Ha, Origin of the slow photoresponse in an individual sol-gel synthesized zno nanowire, Appl. Phys. Lett. 90 (2007) 153106.
[41] W. Guo, S. Xu, Z. Wu, N. Wang, M.M. Loy, S. Du, Oxygen-assisted charge transfer between zno quantum dots and graphene, Small 9 (2013) 3031–3036.
[42] A. Bera, D. Basak, Role of defects in the anomalous photoconductivity in zno nanowires, Appl. Phys. Lett. 94 (2009) 163119.
[43] W. An, X. Wu, X.C. Zeng, Adsorption of o2, h2, co, nh3, and no 2 on zno nanotube: a density functional theory study, J. Phys. Chem. C 112 (2015) 5747–5755.
[44] G. Li, H. Zhang, L. Meng, Z. Sun, Z. Chen, X. Huang, Y. Qin, Adjustment of oxygen vacancy states in zno and its application in ppb-level no2 gas sensor, Sci. Bull. 65 (2020) 1650–1658.
[45] A.K. Elger, J. Baranyai, K. Hofmann, C. Hess, Direct operando spectroscopic observation of oxygen vacancies in working ceria-based gas sensors, ACS Sens. 4 (2019) 1497–1501.
[46] L. Yu, F. Guo, S. Liu, B. Yang, Y. Jiang, L. Qi, X. Fan, Both oxygen vacancies defects and porosity facilitated no2 gas sensing response in 2d zno nanowalls at room temperature, J. Alloy. Compd. 682 (2016) 352–356.
[47] H. Yuan, S.A.A.A. Aljneibi, J. Yuan, Y. Wang, H. Liu, J. Fang, C. Tang, X. Yan, H. Cai, Y. Gu, S.J. Pennycook, J. Tao, D. Zhao, Zno nanosheets abundant in oxygen vacancies derived from metal-organic frameworks for ppb-level gas sensing, Adv. Mater. 31 (2019) 1807161.
[48] J. Zhang, X. Liu, G. Neri, N. Pinna, Nanostructured materials for room-temperature gas sensors, Adv. Mater. 28 (2016) 795–831.
[49] X. Zhou, A. Wang, Y. Wang, L. Bian, Z. Yang, Y. Bian, Y. Gong, X. Wu, N. Han, Y. Chen, Crystal-defect-dependent gas-sensing mechanism of the single zno nanowire sensors, ACS Sens. 3 (2018) 2385–2393.